ARL-TR-9797 ● SEP 2023

DEVCOM ARMY RESEARCH LABORATORY

Structural and Functional Effects of High-Rate Mechanical Loading on Primary Hippocampal Neurons In Vitro

by Ian Berke, Tyson Loudon, and Ann Mae DiLeonardi

NOTICES

Disclaimers

The findings in this report are not to be construed as an official Department of the Army position unless so designated by other authorized documents.

Citation of manufacturer's or trade names does not constitute an official endorsement or approval of the use thereof.

Destroy this report when it is no longer needed. Do not return it to the originator.

ARL-TR-9797 ● SEP 2023

Structural and Functional Effects of High-Rate Mechanical Loading on Primary Hippocampal Neurons In Vitro

Ian Berke, Tyson Loudon, and Ann Mae DiLeonardi
DEVCOM Army Research Laboratory

REPORT DOCUMENTATION PAGE

1. REPORT DATE	2. REPORT TYPE	3. DATES COVERED	
		START DATE	END DATE
September 2023	Technical Report	April 2021	September 2022

4. TITLE AND SUBTITLE
Structural and Functional Effects of High-Rate Mechanical Loading on Primary Hippocampal Neurons In Vitro

5a. CONTRACT NUMBER	5b. GRANT NUMBER	5c. PROGRAM ELEMENT NUMBER
5d. PROJECT NUMBER	5e. TASK NUMBER	5f. WORK UNIT NUMBER

6. AUTHOR(S)
Ian Berke, Tyson Loudon, and Ann Mae DiLeonardi

7. PERFORMING ORGANIZATION NAME(S) AND ADDRESS(ES)
DEVCOM Army Research Laboratory
ATTN: FCDD-RLA-HC
Aberdeen Proving Ground, MD 21005

8. PERFORMING ORGANIZATION REPORT NUMBER
ARL-TR-9797

9. SPONSORING/MONITORING AGENCY NAME(S) AND ADDRESS(ES)	10. SPONSOR/MONITOR'S ACRONYM(S)	11. SPONSOR/MONITOR'S REPORT NUMBER(S)

12. DISTRIBUTION/AVAILABILITY STATEMENT
DISTRIBUTION STATEMENT A. Approved for public release: distribution unlimited.

13. SUPPLEMENTARY NOTES

14. ABSTRACT
Traumatic brain injury is a leading cause of disability and mortality for the modern-day Warfighter. Although progress has been made to diagnose and treat traumatic brain injury, central questions regarding disease initiation and progression remain unanswered. Specifically, directed energy and similar novel exposure paradigms present the potential to influence biology; however, their fundamental mechanisms of action remain unknown and warrant further scientific inquiry. To this end, hippocampal cultures were grown upon various tissue culture substrates for up to 19 days in vitro. Cultures were exposed, using a custom-built test fixture paired to a piezoelectric driver and signal generator, to frequencies between 15 and 80 kHz or a sham stimulus. Subsequent to exposure, gross cell morphology, membrane permeability, and protein localization were assayed via optical methods. Electrophysiological activity was monitored for changes after exposure using glass microelectrode arrays. Results showed no effect of exposure at acute timepoints assayed in this study. This report establishes methods and a generalizable in vitro framework that may add value to directed energy bioeffects studies with relevance to the Warfighter. Future efforts should aim to, more comprehensively, study temporal alterations to cell biology after exposure to a myriad of intelligence informed waveforms.

15. SUBJECT TERMS
Biological and Biotechnology Sciences, neuroscience, brain injury, in vitro, acoustic bioeffects

16. SECURITY CLASSIFICATION OF:			17. LIMITATION OF ABSTRACT	18. NUMBER OF PAGES
a. REPORT	b. ABSTRACT	C. THIS PAGE		
UNCLASSIFIED	UNCLASSIFIED	UNCLASSIFIED	UU	29

19a. NAME OF RESPONSIBLE PERSON	19b. PHONE NUMBER *(Include area code)*
Ian Berke	(410) 273-7722

STANDARD FORM 298 (REV. 5/2020)
Prescribed by ANSI Std. Z39.18

Contents

List of Figures

List of Tables

1. Introduction

Traumatic brain injury continues to create a large socioeconomic burden in civilian and military healthcare. To protect against brain injury, it is necessary to understand the physical and biological mechanisms of injury. However, the research community, following decades of work, still does not understand the relationship between injury mechanics and corresponding biological outcomes. In the early 2000s, most civilian and non-civilian brain injuries were the result of blunt trauma; however, in approximately 2006, blast injury jumped to the forefront of non-civilian brain injury. Now, 15 years later, systems continue to evolve, and Soldiers are being exposed to invisible threats, such as directed energy, with unknown biological consequence. The most fundamental mechanisms that govern injury response following exposure to directed energy remain unknown. This knowledge gap is of great concern and warrants scientific inquiry.

The parameter space of biorelevant RF radiation is vast, making it a large hurdle to quickly assess a wide breadth of candidate sources. However, reported aversive neurosensory symptoms allow us to focus on specific frequencies, intensities, and modulations.[1–4] Field data lack reports of warming sensations or sweating; therefore, we hypothesize that RF radiation in these cases may have low average power densities such that bulk tissue heating remains less than 1° C.[5] Numerous foreign and domestic researchers have demonstrated RF bioeffects without bulk tissue heating. Specifically, sample irradiation with pulsed high-powered microwave (HPM) may illicit the microwave-auditory effect (MAE) and has been shown to produce audible frequencies in several species during pulsed RF exposure.[6] This effect aligns with patient reports of perceived vestibular symptomatology.[7,8]

Rather than exposing cells to pulsed-HPM and relying on the MAE to generate acoustic pressure waves, we propose the use of mechanically driven oscillations with a high frequency shaker. By forgoing electromechanical coupling/transduction (HPM → heat → pressure), we can simplify the experimental paradigm and better monitor cellular response without concern for electromagnetic interference between the source and our unshielded in vitro toolkit. To this end, we utilized a piezoelectric driver to deliver high-frequency, low-magnitude pressure waves to neuronal cultures to better understand their influence in the absence of alternative coupling mechanisms that may occur during pulsed-HPM exposures. Specifically, mixed cultures of neurons and astrocytes were coupled to a high-frequency piezoelectric shaker at varied intensities and repetition rates bounded by prior modeling work. Following, structural and functional measures of cell health were performed to assess the influence of exposure parameters.

2. Methods

2.1 Hippocampal Cultures

Cells were isolated from E18 rat hippocampus (BrainBits, Springfield, IL) using enzymatic digestion as previously described.[9,10] After dissociation, cells were plated on various prepped substrates. Before plating, cell culture substrates were treated with oxygen plasma and polyethylenimine to enhance cell-substrate adhesion. For electrophysiological outcomes, glass microelectrode arrays were used (60MEA200/30iR-Ti; Multi Channel Systems, Reutlingen, Germany); for image-based outcomes, glass bottom 35-mm dishes were used (FluoroDish; Word Precision Instruments, Sarasota, FL); and for membrane permeability assays, tissue culture treated 48-well polystyrene dishes (CellTreat, Pepperell, MA) were used. Cells were seeded at densities of 50,000 to 100,000 cell/cm^2 and media exchanges were performed twice weekly with NbActiv4 (BrainBits) or Neurobasal Medium supplemented with B-27 and Glutamax for up to 19 days in vitro (DIV).

2.2 Piezoelectric Acoustic Shaker (PAS)

To produce in vitro exposures an F7-1 piezoelectric shaker, N8HFS matching network, and PA8HF power amplifier (Wilcoxon Sensing Technologies, Frederick, MD) were used in tandem with a standard signal generator (Fig. 1A). Custom machined aluminum fixtures were designed to couple the piezoelectric shaker head with various standard cell culture vessels. Frequency response was assessed using a vibrometer (VibroFlex Compact; Polytec, Waldbronn, Germany), and frequency content (Fig. 1B) was confirmed using MATLAB R2022a (MathWorks, Natick, MA). To test for a relationship between input parameters (input amplitude and frequency) and measured/calculated outputs (prominence and average velocity), a linear regression was performed (Prism 8.0; GraphPad, San Diego, CA). Statistical significance was set at $p < 0.05$.

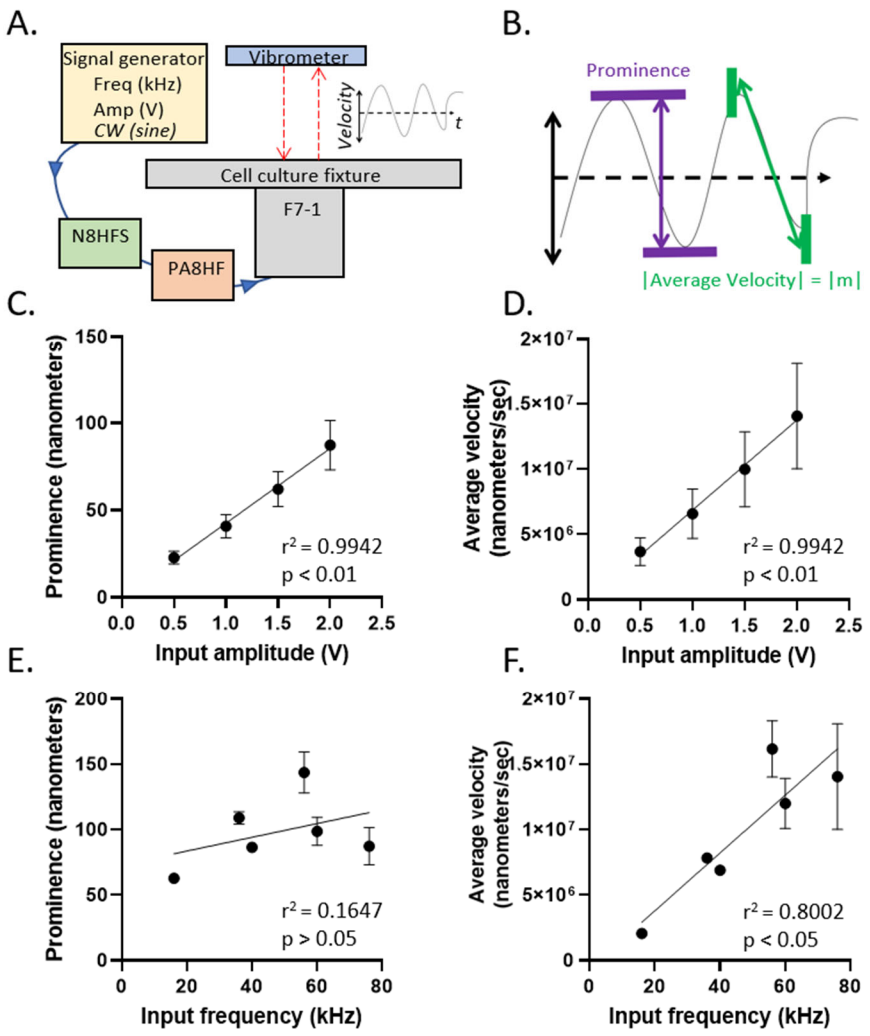

Fig. 1 Validation of piezoelectric shaker. A) Component diagram showing test setup for motion validation and raw velocity measurements collected at 204.8 kHz. B) Data were passed through 1-kHz high-pass filter and integrated to determine position which was used to calculate piezoelectric profile. C) Prominence/stroke and D) average velocity as a function of input voltage with and input frequency of 76 kHz. E) Prominence and F) average velocity across input frequencies with a constant input amplitude of 2 V. Data are presented as mean ± standard deviation (SD).

2.3 Acoustic Exposure Paradigm

A vast parameter space exists within the realm of acoustic exposures. Waveforms utilized in this study were informed by previously described finite element analysis performed by Dagro[4] and colleagues. Modeling and simulation experiments (Appendix, A.2) were bounded within the working range of the F7-1 piezoelectric shaker (1–80 kHz). Cultures were positioned within the test fixture and either exposed to a sham stimulus (negative control) or a frequency sweep where six

distinct frequencies (15, 20, 30, 40, 60, and 80 kHz) were played for 20 s each, at an input amplitude of 2 V. Each exposure lasted for a total duration of 120 s.

2.4 Electrophysiology

To assay electrophysiological activity of primary neuronal cultures, a 128-channel RHS stim/recording controller (Intan Tech, Los Angeles, CA) was used to collect field recordings at 37°C in ambient atmospheric conditions. Data acquisition was accomplished using RHX data acquisition software (version 3.0.2) with a sampling rate of 30 kHz and a 60 Hz notch filter. Baseline field recordings were collected 3 min before sham or PAS exposure. Post-exposure recordings were immediately collected for a total duration of 10 min. Subsequently, cultures were treated with tetrodotoxin ([TTX] 1 μM) for additional field recordings to confirm biological nature of the fields recorded. Spike sorting and subsequent data analysis were performed using NeuroExplorer (version 5.4; Colorado Springs, CO). Briefly, a 4th order band-pass filter (200–3,000 Hz) was applied, spikes that were larger than 5σ from the mean were counted. Spike numbers were then used to calculate firing frequency as a function of recording duration. To test for an effect of treatment, a repeated-measures two-way analysis of variance (ANOVA) was used; TTX data were not included in statistical analyses. Statistical significance was set at $p < 0.05$.

2.5 Membrane Permeability and Image Analysis

A membrane permeability assay to evaluate the development of nanopore formation was performed. Briefly, cells were incubated with fluorescent test compounds (100 μM) of varying hydrodynamic radii (Table 1), exposed to control or acoustic conditions, incubated for 10 min at 37° C, and washed three times with phosphate-buffered saline (PBS) containing calcium and magnesium. Cultures were imaged using a fluorescent plate reader (Infinite F200 Pro; Tecan, Männedorf, Switzerland) and/or inverted microscope (ECLIPSE Ti; Nikon Instruments, Melville, NY) depending on substrate form factor. Additional wells were treated with 0.01% saponin, a surfactant and membrane permeabilizer, to serve as positive control. For quantification of image data, the mean fluorescent intensity within each image field of view was utilized in calculations. For image and plate reader analysis, fluorescent data were normalized to control samples. ImageJ (National Institutes of Health, Bethesda, MD) was used to quantify changes in fluorescent micrographs to detect differences between control and PAS-treated samples, an unpaired Student *t* test was performed when normality and variance test assumptions were met.

Table 1 Test molecules used to determine membrane permeability

Test molecule	Molecular weight (Da)	Stokes radius (nm)	Excitation (nm)	Emission (nm)
Fluorescein	332	0.5	498	517
Propidium iodide (PI)	668	0.6	535	615

2.6 Immunocytochemistry

Immunocytochemistry was used to examine protein localization within cell cultures. Briefly, cells were incubated with 4% paraformaldehyde for 15 min at room temperature, then washed with PBS three times, permeabilized with 0.25% Triton X-100 for 10 min, and blocked with 10% bovine serum albumin for 30 min. Cultures were incubated with the primary antibodies (glial fibrillary acidic protein [GFAP] [ab4674; Abcam, Cambridge, United Kingdom] and microtubule-associated protein 2 [MAP2] [M1406; Sigma-Aldrich, St. Louis, MO] at 1:500) for 1 h, followed by a 1-h incubation with secondary fluorescent antibodies (Alex488-anti-mouse [715-547-003] and Cy5-anti-chicken [703-175-155], 1:250; Jackson ImmunoResearch, West Grove, PA). Images were captured using an inverted microscope (ECLIPSE Ti).

3. Results

3.1 Validation of PAS

The PAS performed as expected, that is, increasing signal generator input voltage resulted in a linear increase in prominence (Fig. 1C, $r^2 = 0.9942$, $p < 0.01$) and average velocity (Fig. 1D, $r^2 = 0.9942$, $p < 0.01$). However, modifying the input frequency while holding the signal generator voltage constant did not result in a linear relationship with respect to prominence (Fig. 1E, $r^2 = 0.1647$, $p > 0.05$). Unsurprisingly, input frequency was linearly related to average velocity when voltage was held constant (Fig. 1F, $r^2 = 0.8002$, $p < 0.05$).

3.2 Qualitative Analysis of Neuronal Morphology and Protein Localization after PAS Insult

Brightfield imaging was used to determine whether PAS exposure resulted in gross morphological changes to co-cultures of neurons and astrocytes. Images captured before PAS exposure in both conditions revealed a confluent bed of cells containing phase-bright neurons with nongranular somas and astrocytes identified by granular somas lacking phase-bright rings (Fig. 2A). Following PAS insult cultures were imaged at the same spatial coordinates (Fig. 2B), neither sham nor PAS cultures

showed evidence of overt cell detachment. Qualitatively, both the sham- and PAS-exposed cultures appear similar to their pre-exposure counterpart (Figs. 2A and 2B). Furthermore, PI staining, indicative of cell death, in PAS-exposed cultures was minimal and similar to that observed in sham cultures, suggesting good overall viability and cell health (Fig. 2C).

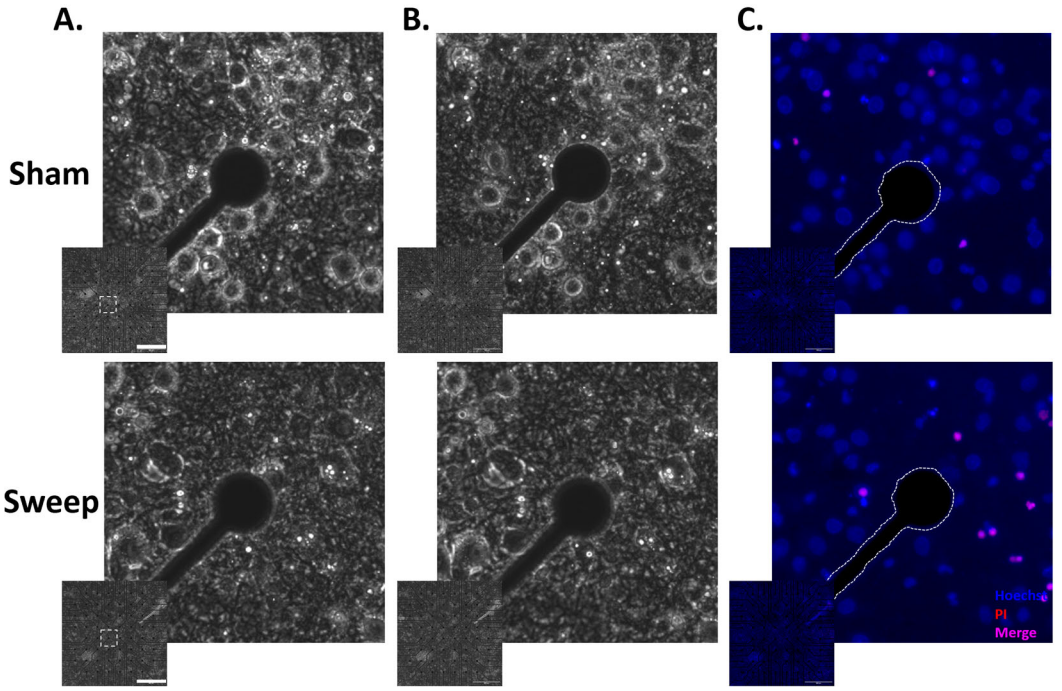

Fig. 2 Wideband acoustic insult does not result in morphological changes or an increase in cell death. Cultures were imaged immediately before A) and after B) exposure to assess changes to morphology. No overt change to Hoechst or PI staining in fluorescent C) images after acoustic exposure (t = 1 h). Scale bar = 500 µm.

Immunostaining for the cytoskeletal-related proteins MAP2 (green) and GFAP (magenta) highlight healthy mixed cultures of neuronal and glial cell types (Fig. 3). Within micrographs from sham- and PAS-treated groups, a relatively dense population of intact neurites can be observed with minimal protein beading or nucleation which has been observed following some traumatic cell injuries.[11,12]

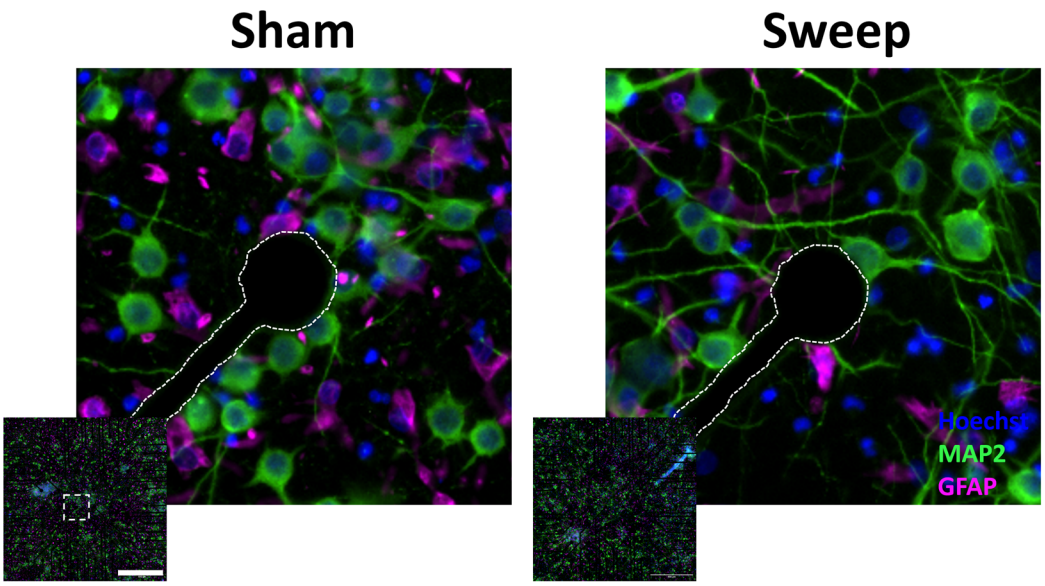

Fig. 3 Wideband acoustic exposure did not alter morphology of neurons (MAP2) or astrocytes (GFAP). After acoustic exposure (t = 1 h), localization of MAP2 and GFAP appear similar, representative immunocytochemistry images are shown. Scale bar = 500 µm.

3.3 Quantitative Analysis of Electrophysiology after PAS Insult

Robust electrical activity was observed in primary cultures at later DIVs and at high seeding densities. Following sham or PAS exposure, electrophysiological signals appeared similar in shape and amplitude (Fig. 4A). TTX treatment resulted in an overt reduction in activity (Figs. 4A and 4C), confirming that field recordings were of biological origin and not simply noise. Quantification revealed that trends in spike frequency (Fig. 4B) remained largely similar across sham and sweep groups, repeated-measures two-way ANOVA revealed a treatment effect ($p = 0.0018$), however, group ($p = 0.20$) and interaction ($p = 0.09$) terms were nonsignificant.

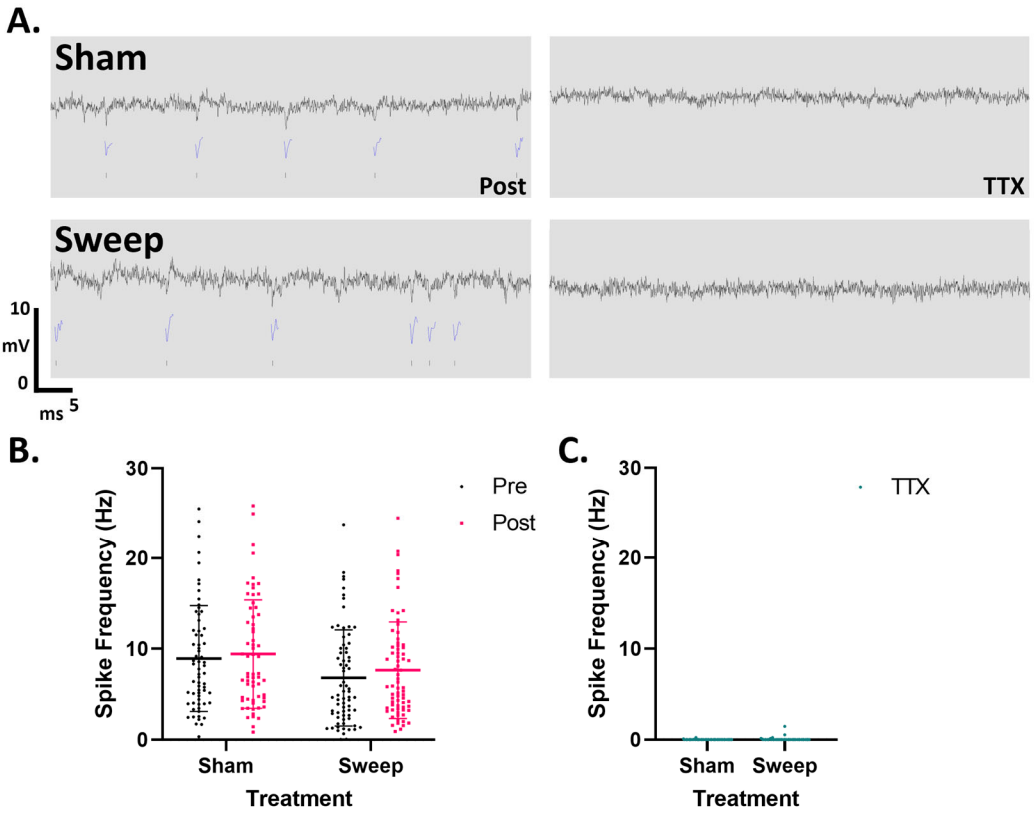

Fig. 4 Spike frequency was not altered after wideband acoustic exposure compared to sham cultures. A) Representative electrophysiology data after sham and wideband acoustic exposure, treatment with TTX shows a robust reduction in bulk electrical activity, verifying the signal measured was from neuronal activity. Differences in spike frequency B) were not detected between sham and wideband sweep exposures; however, treatment with C) TTX showed a robust decrease in activity. Mean ± SD.

3.4 Quantitative Analysis of Membrane Permeability after PAS Insult

Cultures were incubated with different-sized (332 and 668 Da), fluorescently tagged, test molecules which are normally unable to cross cell membranes into the cytoplasm and Hoechst, a fluorescent marker that binds to DNA and can cross phospholipid membranes within viable cells. The appearance of these test molecules following PAS exposure would indicate disruption to the cellular membrane. Imaging analysis revealed that sham- and PAS-exposed cultures exhibited minimal colocalization of either test molecule with Hoechst suggesting largely intact cellular membranes (Fig. 5A). These results were further illustrated by quantifications of imaging data which showed no difference between groups ($p > 0.05$, Fig. 5B). Quantification of the 332 Da test molecule was 1.000 relative fluorescence units (RFUs) for sham and 1.001 RFU for PAS-exposed cultures compared to 1.0187 RFU observed in the saponin-treated positive control.

Quantification of the 668 Da test molecule was 1.153 RFU for sham and 1.171 RFU for PAS-exposed cultures compared to 1.502 RFU observed in the positive control treated with saponin.

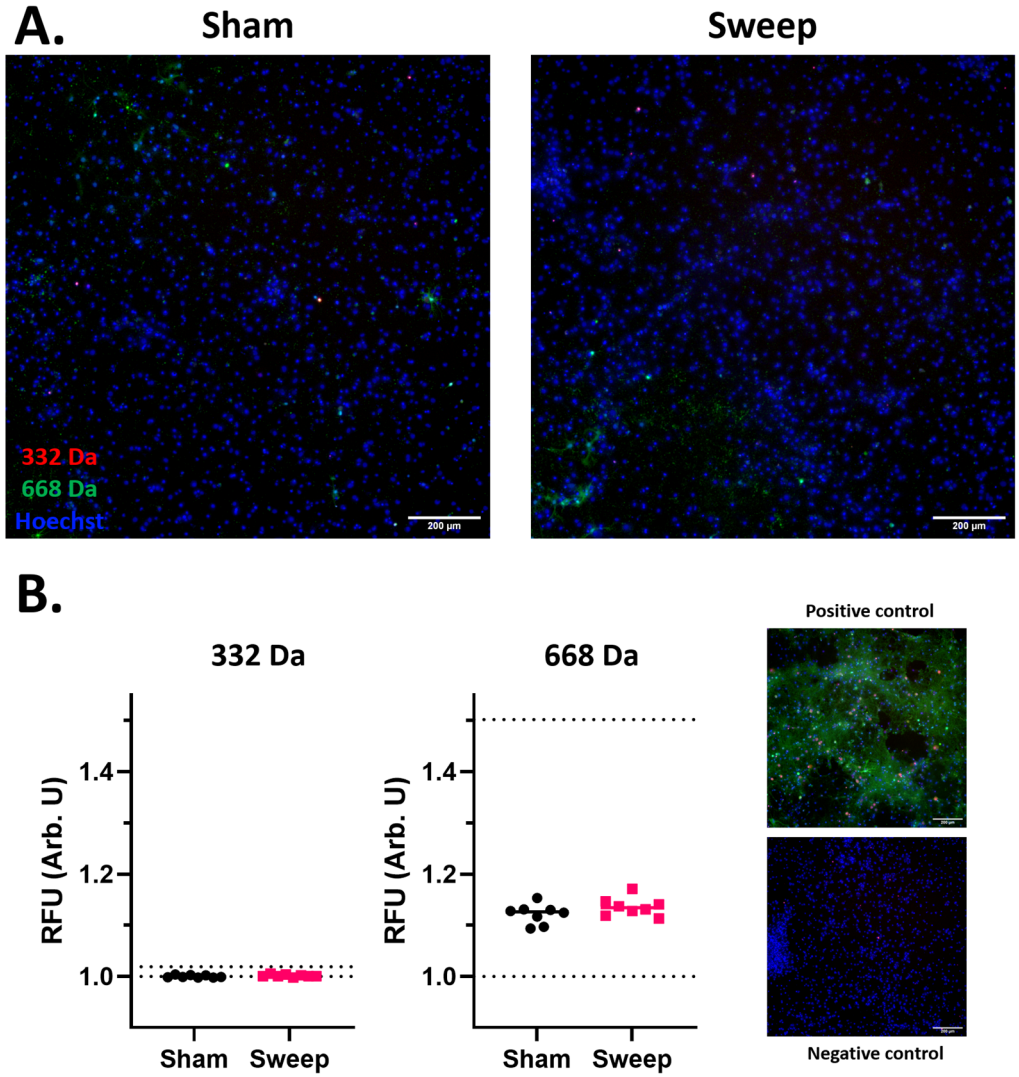

Fig. 5 Wideband acoustic exposure did not influence membrane permeability to test molecules. Representative images A) and quantified fluorescent intensities B) highlight similar levels of 332 and 668 Da test molecule in sham and sweep exposure groups. Dotted lines represent positive and negative control data, respectively. Controls are also shown via the inset images. Scale bar = 200 µm. Arb. U = arbitrary units.

4. Discussion

Within the scope of this technical report, we sought to develop a framework to study the influence of high-frequency, low-magnitude, pressure waves on neuronal cultures. To this end, a variety of biophysical, biochemical, and bioelectrical inquiry techniques were used to investigate changes shortly following acoustic

insult. Cultures largely remained unaltered after acoustic exposure within the parameters explored by this report. Nevertheless, this research serves to establish methods that may add value to future bioeffect studies of pulsed-HPM relevant to the MAE.

In this study a particular interest was taken in developing methods to investigate the combined effect of in situ strain and strain rates. Importantly, it must be noted that bulk elastic properties of brain tissues at ultrasonic frequencies are ~1000 times stiffer than shear properties at lower loading frequencies.[13] These nonlinear, shear thickening, properties have also been demonstrated in single molecule-type rheological studies of lipid fluidity.[14] Given these mechanical properties, it remains feasible that low-strain, high strain-rate loading conditions may elicit changes to cell membrane integrity. Prior work by Geddes et al.[15] demonstrates a consistent transient increase in membrane permeability to fluorescent tracers of various sizes following 30% strain, $10s^{-1}$; however, at lower strain/strain-rate combinations, significant changes in tracer uptake was not observed. Taken together with results presented in this study, it may be inferred that in situ strain/strain-rates experienced during acoustic exposure were relatively low given the lack of observed change in small-molecule fluorescent tracer uptake.

The loss of ionic homeostasis is a hallmark of both mild and severe traumatic brain injury. Acutely, severe traumatic brain injury increased intracellular [K+] and subsequent seizure activity in vivo.[16,17] Similar phenomena have been observed following in vitro injury with increased intracellular ion concentrations following mechanical stretch.[18] Work by Lusardi[19] and colleagues showed significant transient increases to intracellular [Ca2+] at substrate strains as low as 2%, nevertheless, significant cell death was only observed with strains greater than 50% 24 h after injury. Measures of network level electrical activity in brain organotypic cultures, such as network synchronization and spontaneous firing rate, have also been shown to be unchanged at acute and 24-h timepoints following moderate stretch (20%) by Kang[20] and coworkers. We observed no group (sham vs. sweep) or interaction (group*treatment) effects to spike frequency at an acute timepoint after acoustic exposure. These data again support a lack of overt functional alterations to population-level electrophysiological measures shortly following acoustic exposure.

Although this study investigated a comprehensive set of parameters that fell within the workable range of the utilized PAS, there remain several limitations of this work. Namely, higher frequency spectra were not investigated. Recently there has been great interest in the field of mechanobiology in studying mechanisms of mechanotransduction, specifically, how ultrasound may mediate biology. Mechanically triggered channels such as Piezo1 and 2 have been shown to be

directly activated upon exposure to low-intensity (0.1 MPa peak negative pressure) pulsed ultrasound in vitro with a 500 kHz carrier frequency.[21] Furthermore, these specific excitatory effects have been noted in the absence of large thermal excursions in vivo. Interestingly, Chen and colleagues have utilized high-intensity focused ultrasound, and its waveform dependent thermal excursions, to rapidly modulate cellular activity within transient receptor potential cation channel subfamily V member 1 (TRPV1)-overexpressing neurons deep within the brain; somewhat similarly, Konofagou and coworkers have shown an ability to stimulate peripheral nerve in wild-type mice upon exposure to high-intensity focused ultrasound.[22–24] These short-lived excitatory effects were without overt thermal- or pressure-induced injury. These studies, and others, highlight the importance of expanding the frequency content explored in future experiments. In addition to carrier frequency modulation, alternative waveform characteristics such as duty factor and pulse repetition frequency should be considered.

5. Conclusions

In conclusion, this report serves to develop a generalizable framework that can be applied to assay pulsed-HPMs, in addition to other RF spectra, in their relevance to brain injury. It also highlights high-throughput and quantitative techniques to measure biophysical changes in a reproducible primary cell culture system. Future work should aim to, more comprehensively, study the temporal characteristics of cell biology following exposure. Further, techniques to monitor transcriptome and epigenetics may provide additional insight into novel injury mechanisms and potential treatment and mitigation strategies for the Warfighter following exposure to directed energy.

6. References

1. Frey AH, Feld SR. Avoidance by rats of illumination with low power nonionizing electromagnetic energy. J Comp Physiol Psychol. 1975;89:183–188.

2. Sullivan M. Cuba: U.S. Policy in the 115th Congress; 2019. doi:R44822v25.

3. Rubio M, Johnson R, Flake J, Gardner C, Isakson J, Cardin B, Udall T, Shaheen J, Kaine T. Attacks on U.S. diplomats in Cuba: response and oversight; 2018 [accessed 20 July 2022] https://www.foreign.senate.gov/imo/media/doc/01 09 18 Attacks on US Diplomats in Cuba -- Response and Oversight.pdf.

4. Dagro A, Wilkerson J, Thomas T, Kalinosky B, Payne J. Computational modeling investigation of pulsed high peak power microwaves and the potential for traumatic brain injury. Sci Adv. 2021;7:eabd8405. doi:10.1126/sciadv.abd8405.

5. Golomb BA. Diplomats' mystery illness and pulsed radio frequency/microwave radiation. Neural Comput. 2018;30:2882–2985.

6. Frey AH, Messenger R. Human perception of illumination with pulsed ultrahigh-frequency electromagnetic energy. Science. 1973;181:356–358.

7. Whitney SL, Hoppes CW, Lambert KH, Klatt BN. Physical therapy treatment of a person exposed to directed energy: a case report. Mil Med. 2022;187:e1487–e1493.

8. Hoffer ME, Levin BE, Snapp H, Buskirk J, Balaban C. Acute findings in an acquired neurosensory dysfunction. Laryngoscope Investig Otolaryngol. 2019;4:124–131.

9. DiLeonardi AM. Establishing a protocol to culture primary hippocampal neurons. Army Research Laboratory (US); 2020. Report No.: ARL-TR-8900.

10. Banker GA, Cowan WM. Rat hippocampal neurons in dispersed cell culture. Brain Res. 1977;126:397–425.

11. Monnerie H, Tang-Schomer MD, Iwata A, Smith DH, Kim HA, Le Roux PD. Dendritic alterations after dynamic axonal stretch injury in vitro. Exp Neurol. 2010;224:415–423.

12. Johnson VE, Stewart W, Smith DH. Axonal pathology in traumatic brain injury. Exp Neurol. 2013;246:35–43.

13. Lippert SA, Rang EM, Grimm MJ. The high frequency properties of brain tissue. Biorheology. 2004;41:681–91.

14. Espinosa G, López-Montero I, Monroy F, Langevin D. Shear rheology of lipid monolayers and insights on membrane fluidity. Proc Natl Acad Sci. 2011;108:6008–6013.

15. Geddes DM, Cargill RS, LaPlaca MC. Mechanical stretch to neurons results in a strain rate and magnitude-dependent increase in plasma membrane permeability. J Neurotrauma. 2003;20:1039–1049.

16. Takahashi H, Manaka S, Sano K. Changes in extracellular potassium concentration in cortex and brain stem during the acute phase of experimental closed head injury. J Neurosurg. 1981;55:708–717.

17. Morrison B, Saatman KE, Meaney DF, Mcintosh TK. In vitro central nervous system models of mechanically induced trauma: A review. J Neurotrauma. 1998;15:911–928.

18. Wolf JA, Stys PK, Lusardi T, Meaney D, Smith DH. Traumatic axonal injury induces calcium influx modulated by tetrodotoxin-sensitive sodium channels. J Neurosci. 2001;21:1923–1930.

19. Lusardi TA, Wolf JA, Putt ME, Smith DH, Meaney DF. Effect of acute calcium influx after mechanical stretch injury in vitro on the viability of hippocampal neurons. J Neurotrauma. 2004;21:61–72.

20. Kang WH, Cao W, Graudejus O, Patel TP, Wagner S, Meaney DF, Morrison B. Alterations in hippocampal network activity after in vitro traumatic brain injury. J Neurotrauma. 2015;32:1011–1019.

21. Qiu Z, Guo J, Kala S, Zhu J, Xian Q, Qiu W, Li G, Zhu T, Meng L, Zhang R, Chan HC, Zheng H, Sun L. The mechanosensitive ion channel piezo1 significantly mediates in vitro ultrasonic stimulation of neurons. iScience. 2019;21:448–457.

22. Kubanek J, Shukla P, Das A, Baccus SA, Goodman MB. Ultrasound elicits behavioral responses through mechanical effects on neurons and ion channels in a simple nervous system. J Neurosci. 2018;38:3081–3091.

23. Yang Y, Pacia CP, Ye D, Zhu L, Baek H, Yue Y, Yuan J, Miller MJ, Cui J, Culver JP, Bruchas MR, Chen H. Sonothermogenetics for noninvasive and cell-type specific deep brain neuromodulation. Brain Stimul. 2021;14:790–800.

24. Downs ME, Lee SA, Yang G, Kim S, Wang Q, Konofagou EE. Non-invasive peripheral nerve stimulation via focused ultrasound in vivo. Phys Med Biol. 2018;63:035011.

Appendix. Modeling of Biological Material Coupled to a Piezoelectric Shaker

A.1 Introduction

Within this appendix we describe a numerical model of a cell monolayer affixed to a substrate that is displaced sinusoidally in the vertical direction. Specifically, we attempt to determine whether there are specific frequencies of oscillation to which the material may be sensitive.

A.2 Modeling

The monolayer of cells is modeled as a two-dimensional homogeneous isotropic bulk elastic material. The elastic material parameters used were $\mu = 1$ kPa and $\lambda = 2$ GPa, where μ and λ are the shear modulus and Lamé's first parameter, respectively. For this choice of material properties, the material is nearly incompressible and has a Poisson ratio of $\nu = 0.49999975$. For reference, the Poisson ratio of an incompressible material is 0.5. Because many finite element methods for linear elasticity suffer from suboptimal rates of convergence for nearly incompressible material, care must be taken when selecting a finite element method.[1] To overcome this problem, we used a method outlined which is known to be robust in the case of nearly incompressible materials.[2]

The cell height above the base of the plate is assumed to be between 5 and 10 μm. We use 5 μm for the height throughout these simulations. Since the culture plate itself is on the order of centimeters (multiple orders of magnitude larger length scale), a choice was made to use periodic boundary conditions on the lateral sides ($x = \pm 1$) of the domain. Hence, this model is essentially uniaxial, and variations are only expected in the vertical direction. Sinusoidally varying displacement boundary conditions are implemented at the base of the plate ($y = 0$) using an angular frequency of ω. Finally, the top of the cell monolayer ($y = 5$) is treated as a free surface (zero traction boundary condition). A diagram of the model and a coarse mesh are shown in Fig. A-1. Note that the mesh is only shown for reference, and in actual calculations a more refined mesh is used.

[1] Ainsworth M, Parker C. Unlocking the secrets of locking: Finite element analysis in planar linear elasticity. Comput Methods Appl Mech Eng. 2022;395.

[2] Arnold DN, Lee JJ. Mixed methods for elastodynamics with weak symmetry. SIAM J Numer Anal. 2014;52:2743–2769.

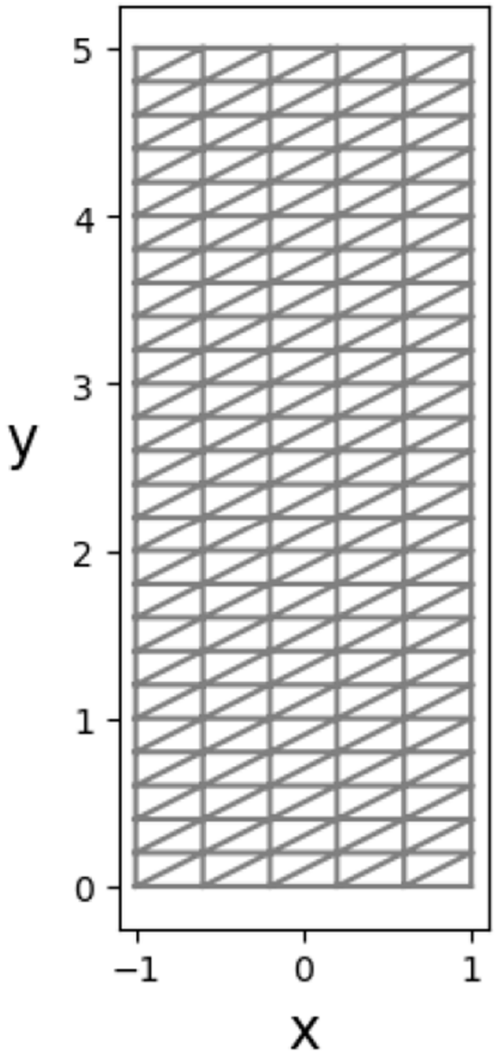

Fig. A-1 Model geometry with dimensions used

In total, there are six model parameters that may be adjusted (Table A-1). Three are material properties including density, shear modulus, and Lamé's first parameter. Two are related to the oscillations applied to the base of the model. These include the angular frequency and amplitude of the sinusoidal oscillations. Lastly, the height of the biological material (cell monolayer) must be specified. One may also consider the width of the domain a parameter to be specified, however, because periodic boundary conditions are used on the lateral sides of the domain, the domain width does not alter the outcome of the simulations. Another consideration in finite element modeling is the size of the time step, the number of triangles/quadrilaterals to use in discretization of the domain, as well as the degree of polynomials used in the approximation. These topics are not discussed for the sake of brevity. We only mention that these issues have been considered, and we believe the numerical results to be sufficiently accurate. Another choice available is the units of

measurement. For this problem we use microns, nanograms, and milliseconds for length, mass, and time, respectively. We remark that in this unit of measurement, pressures are equivalent to the Pascal.

Table A-1 Model parameters used in numerical simulations

Parameter	Description	Value used (SI units)	Value used (μm-ng-ms)
ρ	Density	1.0×10^3 kg/m^3	1.0×10^{-3} ng/μm^3
μ	Shear modulus	1.0×10^3 Pa	$1.0 \times 10^3 \frac{\text{ng}}{\mu\text{m ms}^2}$
λ	Lamé parameter	2.0×10^9 Pa	$2.0 \times 10^9 \frac{\text{ng}}{\mu\text{m ms}^2}$
ω	Angular frequency	46.0×10^3 rad/s	46 rad/ms
α	Amplitude of oscillations	5.0×10^{-7} m	0.5 μm
H	Cell height	5.0×10^{-6} m	5 μm

A.3 Results

In this section, we give the results of finite element simulations using the model parameters presented in Table A-1. The finite element discretization was implemented using the FEniCS software environment.[3]

The finite element model was run for 10 μs and evaluate the von Mises stress along the centerline (x = 0) at three different time values, t = 1, 5, and 10 ms. From these data (Figs. A-2A and A-2B) it is apparent that as time increases, stress accumulates at the base of the plate and decreases linearly to the top surface. Heuristic reasoning, assuming the material is perfectly incompressible, that is, $\lambda \to \infty$, based on separation of variables and D'Alembert's solution to the one-dimensional wave equation suggests that the stress behaves like

$$\sigma \sim \frac{a\omega}{c} t(H - y) \tag{A-1}$$

To verify that this is a consequence of the near incompressibility of the biological material, the simulation was performed again with a Lamé parameter from $\lambda = 2$ GPa to $\lambda = 2$ kPa. These data illustrate that the stress no longer grows linearly in space and time (Figs. A-3A and A-2B) as suggested by (Eq. A-1), rather, von Mises stress shows a more complex behavior that is similar across different values in time. We see a continuous contraction and relaxation of the stress, as one would expect from an elastic solid being sinusoidally displaced. These results should be compared to those presented in Fig. A-2B, which shows that stress increases quasi-linearly in time.

[3]Langtangen HP, Logg A. Solving PDEs in python. Springer; 2017.

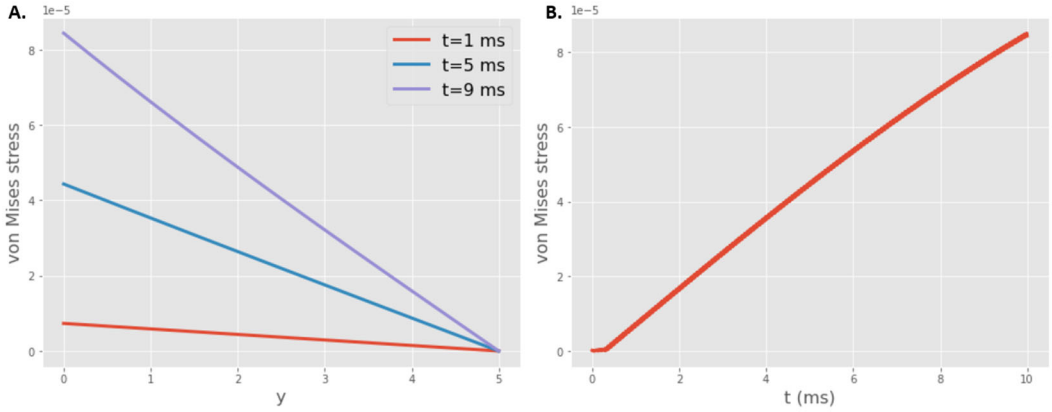

Fig. A-2 A) von Mises stress evaluated at the center line of the model x = 0 and 0 ≤ y ≤ 5 μm for three different time values with λ = 2 GPa and B) the stress evaluated at the point (x, y) = (0, 0) for 0 ≤ t ≤ 10 ms.

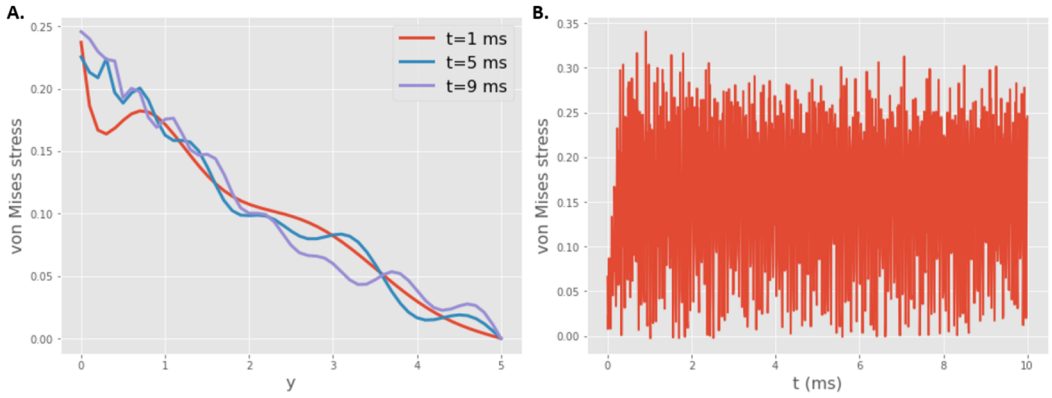

Fig. A-3 A) von Mises stress evaluated at the center line of the model x = 0 and 0 ≤ y ≤ 5 μm for three different time values with λ = 2 kPa and B) the stress evaluated at the point (x, y) = (0, 0) for 0 ≤ t ≤ 10 ms.

A.4 Conclusions

For nearly incompressible material, it does not appear that any "special" frequencies for mechanical insult exist when the insult only involves sinusoidally varying vertical displacement. Instead, as indicated in Fig. A-2A, the material has a fairly predictable response. Namely, the faster and higher you shake the material, the more stress accumulates.

List of Symbols, Abbreviations, and Acronyms

ANOVA	analysis of variance
DIV	days in vitro
GFAP	glial fibrillary acidic protein
HPM	high-powered microwave
MAE	microwave-auditory effect
MAP2	microtubule-associated protein 2
PAS	piezoelectric acoustic shaker
PBS	phosphate-buffered saline
PI	propidium iodide
RF	radiofrequency
RFU	relative fluorescence units
SD	standard deviation
TRPV1	transient receptor potential cation channel subfamily V member 1
TTX	tetrodotoxin

1 (PDF)	DEFENSE TECHNICAL INFORMATION CTR DTIC OCA
1 (PDF)	DEVCOM ARL FCDD RLB CI TECH LIB
3 (PDF)	DEVCOM ARL FCDD RLA HC I BERKE A DILEONARDI T LOUDON